JMEPEG
https://doi.org/10.1007/s11665-024-09667-1

1059-9495/$19.00

ORIGINAL RESEARCH ARTICLE

Synthesis and Characterization Study of $Al_{10}Cr_{25}Co_{20}Ni_{25}Fe_{20}$ High-Entropy Alloy Powders through Mechanical Alloying

D. Jeyasimman, V. Vijayaraghavan, and Sri Venkateshwara

Submitted: 2 November 2023 / Revised: 3 May 2024 / Accepted: 9 May 2024

$Al_{10}Cr_{25}Co_{20}Ni_{25}Fe_{20}$ high-entropy alloys (HEA) with ultrafine grains was synthesized through 30 h of mechanical alloying (MA). The morphological study of prepared high-entropy alloy powders was done by using scanning electron microscope images. Crystallite size and lattice strain of prepared high-entropy alloy were investigated through x-ray diffraction technique. Consolidation and sintering of HEA powders done by two methods such as conventional sintering and spark plasma sintering methods at 1000° and 1200 °C. After 30 h of MA, crystallite size 44 nm and lattice strain 0.182 was obtained. The mechanical properties analysis of high-entropy alloy was done in terms of its density, hardness measurements and compression test. For conventional sintering, the hardness values of 135 ± 6 $HV_{0.5}$ for 1000 °C and 186 ± 8 $HV_{0.5}$ for 1200 °C were obtained. For spark plasma sintering, the hardness values of 167 ± 5 $HV_{0.5}$ for 1000 °C and 212 ± 6 $HV_{0.5}$ for 1200 °C was obtained. Ultimate compressive strength for conventional sintering at 1000 °C and 1200 °C was 246 ± 5 MPa and 305 ± 6 MPa. Ultimate compressive strength of HEA for spark plasma sintered composite at 1000 °C and 1200 °C was 369 ± 5 MPa and 442 ± 5 MPa and the total elongation was 17.7%. BCC and FCC biphase mixture was obtained and confirmed by transmission electron microscopy images and electron backscattered diffraction analysis.

Keywords compressive strength, hardness, high entropy alloy, spark plasma sintering

1. Introduction

The high-entropy alloys (HEAs) have been developed since 2004 (Ref 1, 2), the alloy consists of four or more than four principal elements in equal or nonequal molar concentration. In developing of HEAs, body-centered cubic (BCC) and face-centered cubic (FCC) solid solutions are formed due to combination of multiple principal elements (Ref 3-5). High-entropy alloys were prepared by induction melting, and arc melting (Ref 6, 7) method was reported by earlier studies. Microhardness and wear resistance of Al0.25CoCrFeNiSi0.6 high-entropy alloy prepared by induction melting was studied by Samoilova et al (Ref 6). The effect of Ce addition on purification and inclusion modification mechanism of equiatomic CoCrFeNiMn high-entropy alloy prepared by arc melting was reported by Yin et al (Ref 7). The powder metallurgy route has increased for synthesizing HEAs with excellent mechanical properties (Ref 8-12). Zhou et al. investigated Fe-Cr-Ni-Al-Ti ferritic super alloy fabricated by powder metallurgy and reported that HIP consolidation gave prior particle boundaries (Ref 8). The thermal stability and oxidation behavior of powder metallurgical FeCrNiAl-based medium entropy alloys at 800-1000 °C were investigated by Yang et al (Ref 9). In addition, Rogacheve et al (Ref 10) studied the long-term stability (up to 204 days) of mechanical alloyed CoCrFeNiTi high-entropy alloy at 873, 1073 and 1273 K. AlCoCrFeNiTiZn high- entropy alloy was fabricated by mechanical alloying and followed by sintering in tube furnace with controlled atmosphere by H. Kalantari et al.(Ref 11). They reported that BCC and FCC solid solution was obtained after 120 h of mechanical alloying. Comparative study of the microstructure and phase evolution of FeCoCrNiAl high-entropy alloy-matrix with WC nanocomposite powders prepared by mechanical alloying was investigated by Cheng et al (Ref 12). They reported that after 10 h of MA, BCC gradually transformed to FCC phase and up to 100 h of MA, both BCC and FCC biphasic HEAs were formed.

Recently, mechanical alloying (MA) and followed by spark plasma sintering (SPS) is one of the promising method to develop HEAs with excellent mechanical properties(Ref 13-19). AlCrCuMnNi high-entropy alloy was produced by mechanical alloying and followed by spark plasma sintering at different temperature by Toroghinejad et al(Ref 13). They reported that the hardness, density, and wear resistance increased with increasing spark plasma sintering temperatures due to the sintering quality and formation of intermetallic compounds. Similar results were obtained by Karimi et al (Ref 14) for CoCuFeMnSi high-entropy alloy fabricated by mechan-

D. Jeyasimman, Department of Mechanical Engineering, Periyar Maniammai Institute of Science & Technology, Thanjavur, Tamil Nadu 613 403, India; and The office of the Research & Development, Periyar Maniammai Institute of Science & Technology, Thanjavur, Tamil Nadu 613 403, India; and **V. Vijayaraghavan** and **Sri Venkateshwara**, Department of Mechanical Engineering, Periyar Maniammai Institute of Science & Technology, Thanjavur, Tamil Nadu 613 403, India. Contact e-mails: directorar@pmu.edu and jeyasimman76@gmail.com.

Published online: 07 June 2024

ical alloying and followed by spark plasma sintering. They obtained average crystallite size of 21 nm HEA powder with FCC solid solution after 50 h of MA and improved density, hardness, wear resistance and magnetic properties. Light weight refractory high-entropy alloy $TiAlV_{0.5}CrMo$ was fabricated by mechanical alloying and spark plasma sintering by Cao et al (Ref 15). A BCC solid solution was obtained after milling 30 h of MA and ultra-high hardness and high compressive strength was achieved. FeCrCoNiCu high-entropy alloy was successfully fabricated through 50 h of MA and spark plasma sintering by Toroghinejad et al.(Ref 16). FCC and BCC dual phase solid solution of HEAs was obtained after 50 h and also ultimate shear strength of 300 MPa, and ultimate tensile strength of 540 MPa was achieved. Jain et al. (Ref 17) have synthesized $Fe_{40}Mn_{14}Ni_{10}Ti_{10}Al_{15}Si_{10}$ high-entropy steel through mechanical alloying and spark plasma sintering and major FCC phase and minor BCC phase were obtained. They obtained good mechanical properties such as microhardness 10.4 GPa and ultimate compressive strength 209 GPa. $Ni_{28}Co_{26}Cr_{26}Al_{10}Si_{10}$ high-entropy alloy was synthesized by mechanical alloying and spark plasma sintering by Shahbazkhan et al. (Ref 18). Formation of FCC phase was obtained after 40 h of MA. Olejarz et al. (Ref 19) have been fabricated CoCrFeNi high-entropy alloy with low ball to powder ratio 5:1 through mechanical alloying and followed by spark plasma sintering. Dissolution of Cr-rich phase in the matrix was observed and 3.69 GPa microhardness was obtained. In the recent years, four families of HEAs have been developed, such as 3D transition metals, light weight materials, lanthanides and refractory (Ref 20). AlCrCoNiFe HEAs come under the 3D transition metals family. From that Fe, Co, Cr and Ni are core 3D transition metals whereas Al is light weight metal.

In this attempt, $Al_{10}Cr_{25}Co_{20}Ni_{25}Fe_{20}$ HEA was synthesized by 30 h of MA and morphological and characterization study through XRD, SEM and TEM analysis. The mechanical properties analysis of prepared high-entropy alloy was done by using density, hardness measurements and ultimate compressive strength measurement.

2. Experimental Methods

Aluminum 99% purity and 325 mesh size (40 microns), chromium 99% purity and 100 mesh size, cobalt 99% purity and 100 mesh size, nickel 99.5% purity and 100 mesh size and iron with 99.5% purity and 100 mesh size were purchased from SRL, Mumbai and was used as raw materials for synthesis of HEAs powders. High-energy ball milling machines with tungsten carbide vials and balls were utilized. Ball milling procedure was interrupted every 20 min and halted for 10 min to avoid overheating of vials. Toluene was used as process control agent and the ball-to-powder ratio was 10:1. Toluene or Methanol was used as process control agent in the previous studies. Based on the literature review, in this research work, Toluene was used as a process control agent.

The materials were milled in a highly pure wet agent (Toluene) to avoid the formation of intermetallic compounds during milling. Moreover, toluene minimizes the contamination of powders during long hours of milling.

The milled powders were taken as milled samples at 0, 5, 10, 20 and 30 h interval time for characterization study. The characterization study of as received five pure powders and prepared high-entropy alloy powders (0, 5, 10, 20 & 30 h) was done by using Scanning Electron Microscope (SEM, JEOL – Japan -JSM) images. Crystallite size and lattice strain and dislocation density of prepared high-entropy alloy were investigated through x-ray Diffraction technique (XRD, Rigaku Ultima III XRD). The morphology of powder was examined by bright field image and selected area pattern of transmission electron microscopic (TEM, JEOL JEM 2100 HRTEM) images of 30 h milled powder of HEA.

The as-milled powder after 30 h of MA was consolidated and sintered by two methods such as conventional sintering and spark plasma sintering (SPS) at 1000° and 1200 °C. For conventional sintering, the as-milled powders were cold pressed in a steel die using 50 kN force to obtain cylindrical samples of 10 mm diameter and 15 mm height. The compressed samples were sintered in tubular furnace in argon atmosphere at 1000° and 1200 °C for 3 hrs. For spark plasma sintering, as-milled powders were sintered at 1000° and 1200 °C. The spark plasma sintering (SPS) was done in a graphite die with the holding temperatures 1000° and 1200 °C, and holding time 10 min and uniaxial pressure of 50 MPa, respectively. After 30 h of milling, the powders were compacted using spark plasma sintering (Dr. Sinter, Modal SPS-625, SPS Syntex Inc.). at 1200 and 1400 °C with a heating rate of 100 °C /min and an applied load of 50 MPa and hold time of 10 min (600 s) at the maximum temperature. The size of SPSed samples after sintering was 25 mm diameter and 10 mm height. The heating cycle diagram for spark plasma sintering is shown in Fig. 1. The densities of both methods of sintered samples were measured with a density measuring setup according to Archimedes principle using water as the suspending medium. The theoretical density was calculated as 6.642 g/cm^3 by rule of mixture. Vickers microhardness testing was done with load 500 g and dwell time 10 s. Ultimate compressive strength of prepared high-entropy alloy composite are investigated using universal testing machine – 50 kN.

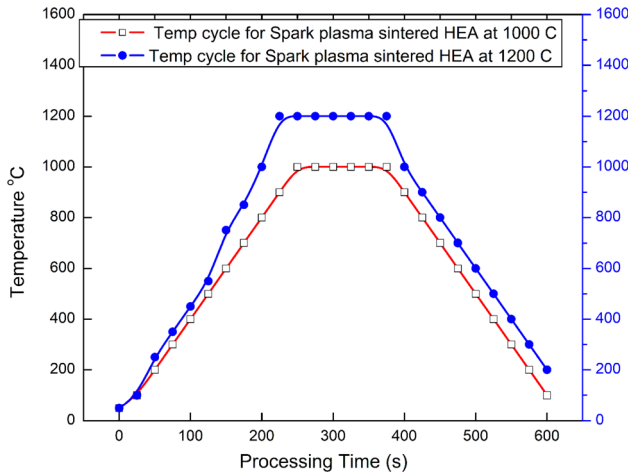

Fig. 1 Heating cycle diagram for spark plasma sintering

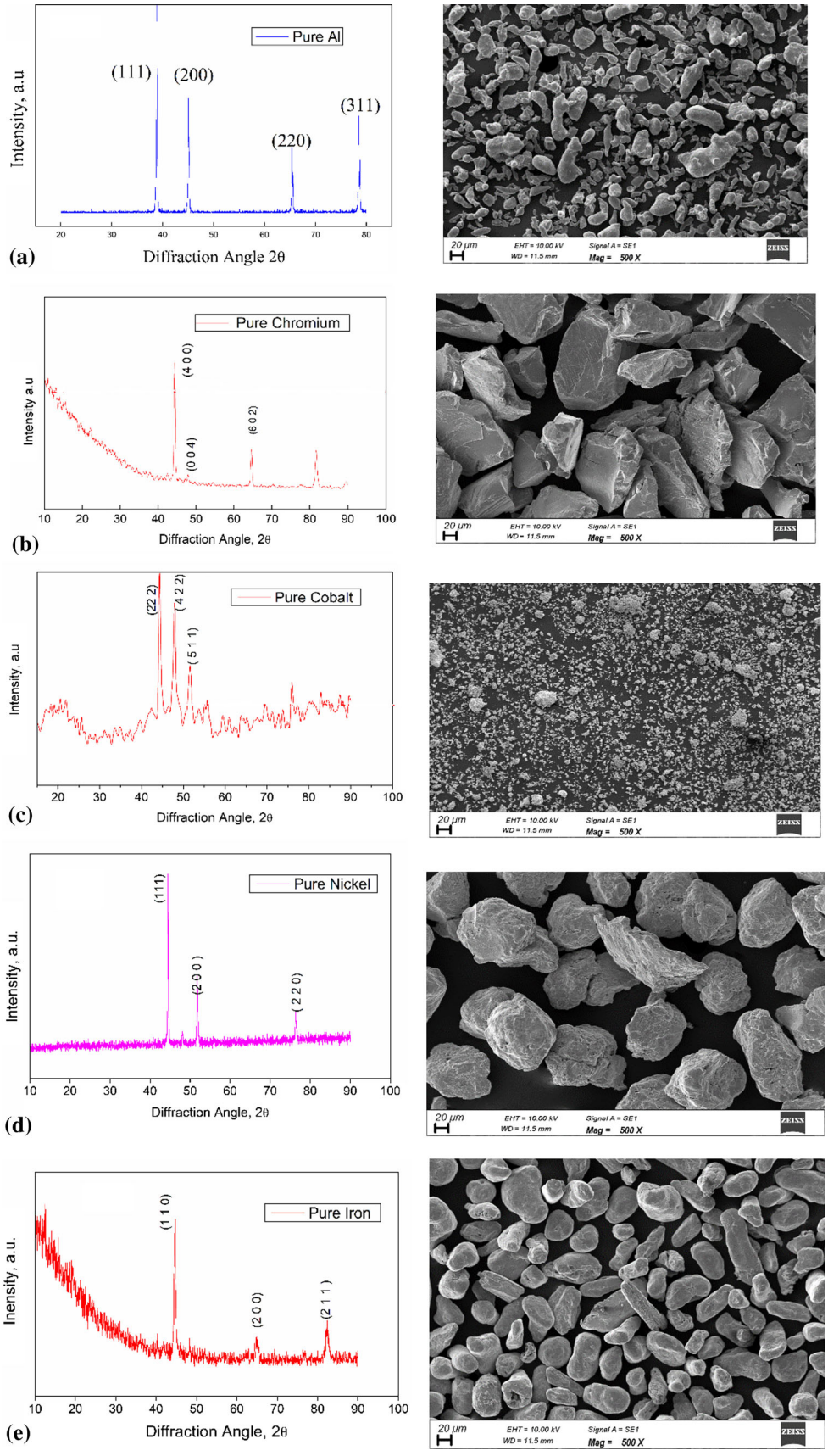

Fig. 2 XRD and SEM images of Pure received powders (a) Al; (b) Cr; (c) Co; (d) Ni and (e) Fe

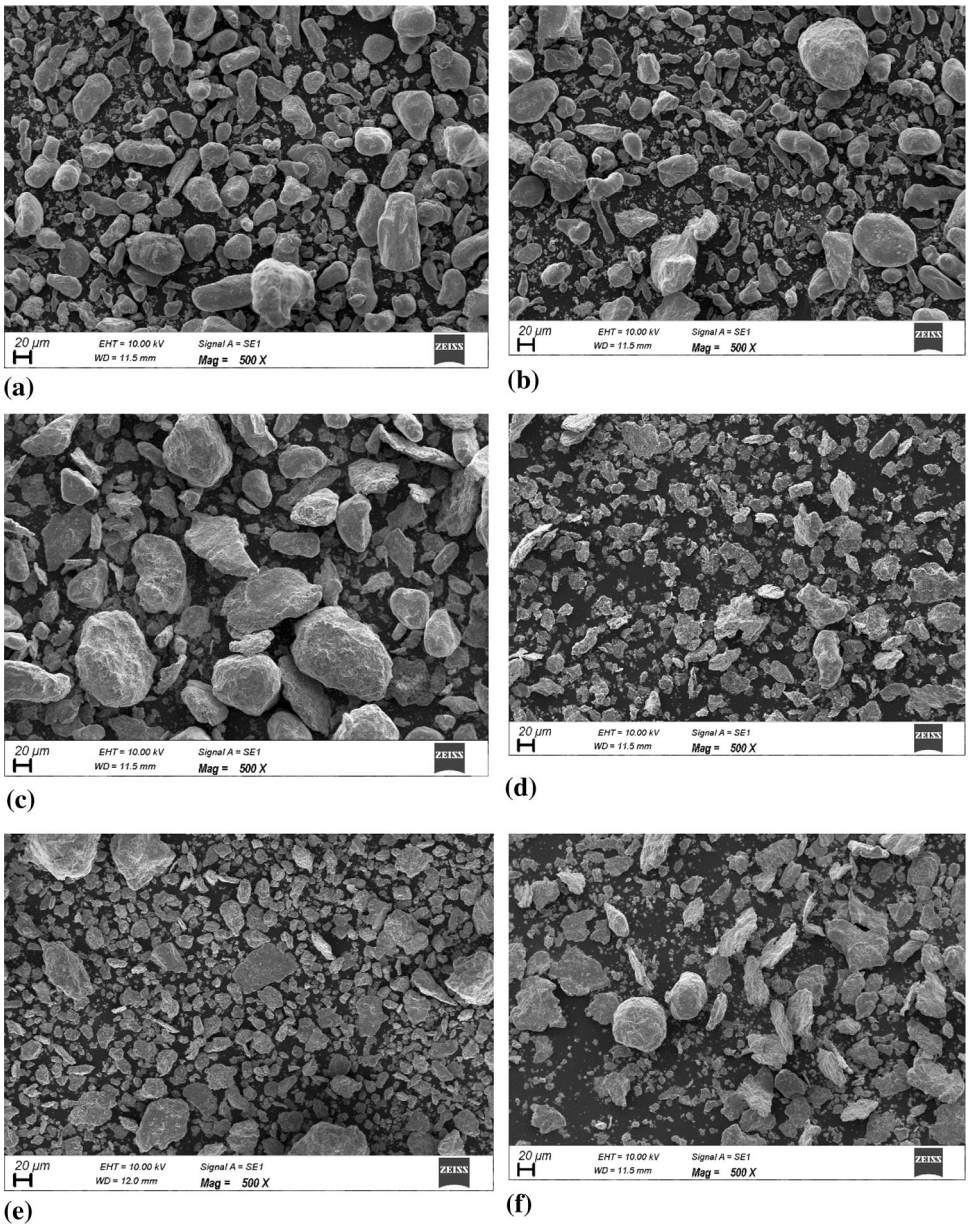

Fig. 3 The morphology of $Al_{10}Cr_{25}Co_{25}Ni_{25}Fe_{20}$ High-entropy alloy (HEAs) powder as a function of the milling time after: (a) 0 h, (b) 1 h, particle flattening and fracturing, (c) 5 h, welding predominance, (d) 10 h, fracturing dominance, (e) 20 h, equiaxed particle formation and (f) 30 h, equiaxed particles (steady state)

3. Result and Discussion

3.1 Microstructure Characteristics of As-received and As Milled HEA Powders

Figure 2 shows XRD and SEM images of as-received pure powders. The main peaks of Al, Cr, Co, Ni and Fe powders were obtained. For aluminum first four peaks (1 1 1), (2 0 0), (2 2 0) and (3 1 1) were obtained. (4 0 0), (0 0 4) and (6 0 2) peaks were obtained for pure chromium powders. For Cobalt (2 2 2), (4 2 2) and (5 1 1) peaks and for nickel (1 1 1), (2 0 0) and (2 2 0) peaks were obtained. For gamma phase iron (1 1 1), (2 0 0) and (2 1 1) peaks were obtained. Scanning electron images of pure powders of Al, Cr, Co, Ni and Fe powders show that all powders are spherical shape and also confirmed the particle size less than 40 microns. Figure 3 shows the morphology of $Al_{10}Cr_{25}Co_{25}Ni_{25}Fe_{20}$ high-entropy alloy (HEAs) powder as a function of the milling time. Before milling, all powders were blended with correct proportions and as considered as 0 h milled powders (Fig. 3a). After 1 h of MA, the powder particles were flattened and fracturing was stated (Fig. 3b). After 5 h of MA, cold welding of powder particles dominates (Fig. 3c). Fracturing was dominant after 10 h of MA (Fig. 3d). Equiaxed particle formation was started after 20 h of MA (Fig. 3e) and after 30 h of MA, almost all particles were formed as equiaxed particles and steady state was attained (Fig. 3f). Figure 4(a) shows XRD patterns of Al10Cr25Co20Ni25Fe20 high-entropy alloy powders after 0, 5, 10, 20 and 30 h of MA. After 30 h of MA, BCC and FCC phases were obtained and shown in figure. Chromium and Iron has BCC crystal structure, whereas Ni and Al has FCC crystal structure. Cobalt has HCP and FCC crystal structure. After 10 h of ball milling, a body-centered cubic

(BCC) phase is obtained. With a further increasing ball milling time, repeated plastic deformation, fracturing and cold-welding of powder particles, the BCC phase gradually transforms into a face-centered cubic (FCC) phase. After 30 h of MA, almost equiaxed and spherical powder particles were obtained and final FCC and BCC biphasic HEA powder was synthesized. Adding element with large atomic radius differences including Al and Ti in HEAs can induce phase transformation. It is noted that, BCC structured HEAs has remarkable strength and hardness when compared to FCC-based HEAs (Ref 21). Zhang et al. (Ref 22) showed the phase transformation from FCC to BCC by increasing Al content in CoCrFeNiAlx HEA and also decreasing the density of HEAs. In this study, after 30 h of MA, for 2θ value 38.3°, Aluminum (FCC) peak (1 1 1) , for 46.9°, chromium peak (0 0 4), for 48.7°, cobalt peak (4 0 2) and for 65°, α Iron peaks (4 4 0) were obtained. In XRD of pure powder, some of peaks were obtained related to Al, Cr, Co, Ni and Fe. After 30 h of MA, there is a formation of multi-component alloy solid solution. Hence, some peaks of metals powders were diminished and dissolved in other metal powders. Moreover, BCC and FCC mixed phase was obtained in the 30 h of milled powders. This was confirmed by obtained results in XRD and EBSD images.

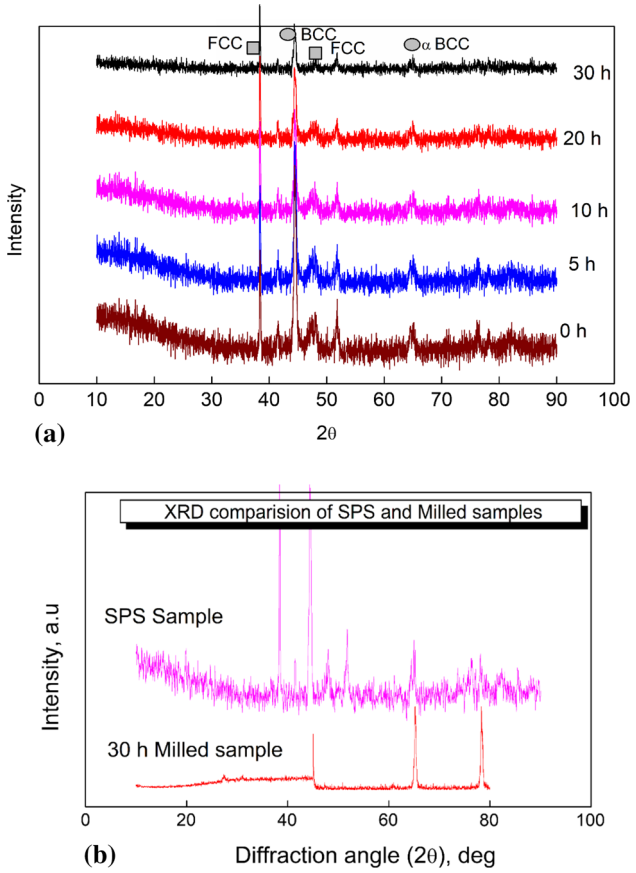

Fig. 4 (a) XRD patterns of $Al_{10}Cr_{25}Co_{20}Ni_{25}Fe_{20}$ High-entropy alloy powders after 0, 5, 10, 20 and 30 h of MA and (b) XRD comparison of milled powder and SPS sintered sample

Table 1 Thermodynamic parameters of prepared HEAs

Sl. no.	Thermodynamic parameters	Value
1	Melting temperature, T_m K	1530 K
2.	Change in mixing enthalpy (ΔH_{mix}), kJ/mol	− 4.01
3.	Change in mixing entropy (ΔS_{mix}), J/k.mol	13.36
4.	VEC	7.6
5.	Phase	BCC + FCC

Valence electron concentration (VEC) is the important thermodynamic parameter for the prediction of solid solution of HEA phases. The thermodynamic parameters such as melting temperature, change in mixing enthalpy and entropy, valence electron concentration (VEC) and phase changes for the formation of solid solution is given in Table 1. The formation of mixed phases consisting of BCC and FCC was verified by the XRD results $6.8 < \text{VEC} < 8.0$ (Ref 13, 23). Based on the XRD results, the formation of BCC and FCC mixed phases was confirmed.

Figure 4(b) shows the comparison of XRD patterns of 30 h MA powder and SPS sample. For both milled powder and SPS sample, three peaks were obtained. First peak at 46.9° is related to Aluminum -FCC peak (1 1 1), second peak related to Cobalt -hcp peak at 65° (4 0 2) and third peak related to Iron -BCC peak at 77° (4 4 0). Other peaks were diminished due to formation of solid solution.

Crystallite size and lattice strain were calculated based on Williamson–Hall Method (Ref 24). The crystallite size (t) and lattice strain (ε) were determined using the standard Williamson–Hall analysis.

$$\beta_{hkl}.\cos\theta_{hkl} = \left[\frac{k\lambda}{t}\right] + 4\varepsilon.\sin\theta_{hkl}$$

where k is the shape factor (0.9), λ is the wavelength of the x-ray (1.5406), θ_{hkl} is the Bragg angle, t is the crystallite size normal to the reflecting planes and ε is the lattice/microstrain. The instrumental broadening corrected line profile breadth, β_{hkl}, was calculated as a full width at half maximum (FWHM) by the computer software (XRD-analyzer) based on each reflection of 2θ. Figure 5(a) shows the change in crystallite size and lattice strain of $Al_{10}Cr_{25}Co_{20}Ni_{25}Fe_{20}$ high-entropy alloy as a function milling time. The crystallite size was gradually decreased and lattice strain was gradually increased up to 10 h of MA and crystallite size was slightly increased and lattice strain was slightly decreased further up to 30 h of MA. Crystallite size was decreased from 265 microns to 44 nm and lattice strain was gradually increased from 0.0562 to 0.182. Similar result was obtained by F.Cao et al (Ref 25). Figure 5(b) shows lattice parameter as function of milling time. Lattice parameter was continuously decreased from 0.492 to 0.345 Å.

3.2 Morphological Study of As Milled HEA Powders

Nanocrystalline phase and phase change was confirmed by bright field image and selected area pattern of transmission

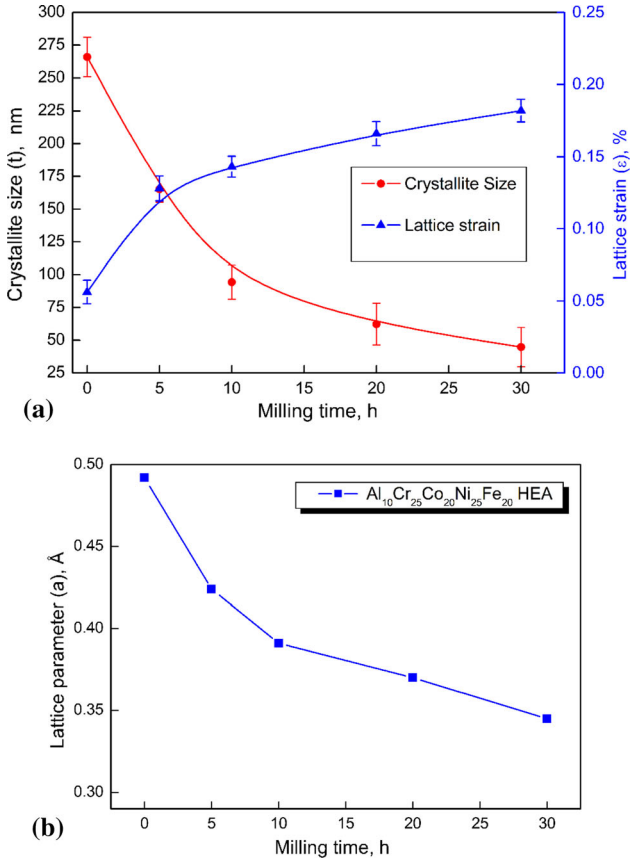

Fig. 5 (a) Change in crystallite size and lattice strain of $Al_{10}Cr_{25}Co_{20}Ni_{25}Fe_{20}$ High-entropy alloy as a function milling time and (b) lattice parameter as function of milling time

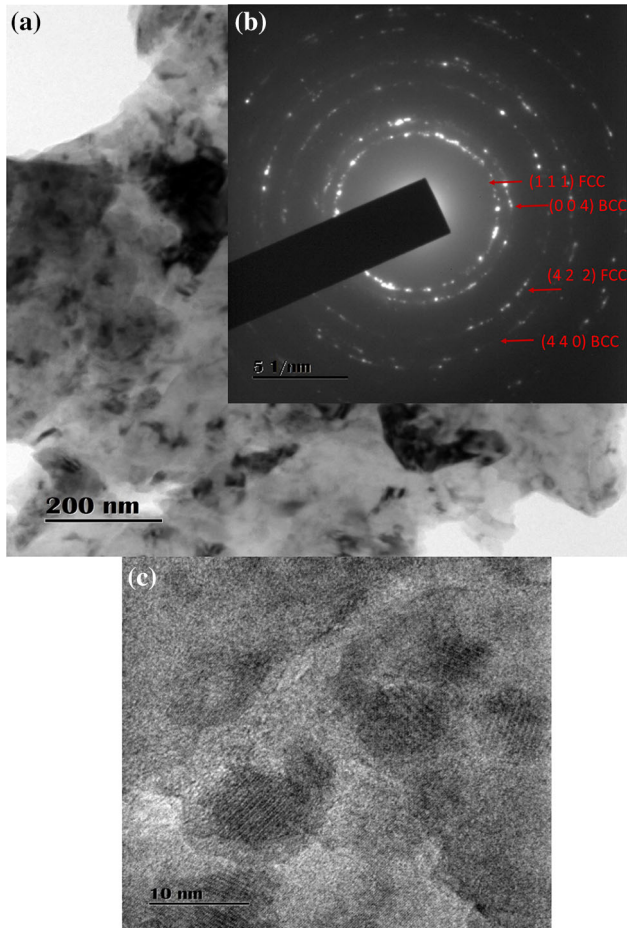

Fig. 6 (a) FETEM bright field image of $Al_{10}Cr_{25}Co_{20}Ni_{25}Fe_{20}$ High-entropy alloy powder after 30 h MA (b) inset the corresponding SAD ring pattern and (c) the corresponding lattice fringes

electron microscopic (TEM) images of 30 h milled powder of HEA. Figure 6(a) shows FETEM bright field image of $Al_{10}Cr_{25}Co_{20}Ni_{25}Fe_{20}$ high-entropy alloy powder after 30 h of MA. Figure 6(b) shows inset the corresponding SAD ring pattern, and Fig. 6(c) shows the corresponding lattice fringes. Similar results were obtained by the previous studies (Ref 12, 15). The results were in good agreement with earlier studies done by B.Ren et al. (Ref 26) and H.Jain et al. (Ref 27). The bright field image and SAD pattern is indexed as BCC and FCC biphase mixture which is in reasonable agreement with the XRD results.

Figure 7 shows the DSC analysis of $Al_{20}Cr_{20}Co_{20}Ni_{20}Fe_{20}$ HEAs 30 h milled powder with heating rate 10 °C min^{-1}. Two exothermic peaks were identified. First peak was obtained at 90 °C, and the second one was obtained at 220 °C. These exothermic peaks were related to crystallization of powders. One endothermic peak was identified at 360 °C, which was related with internal stresses relief. These results are in good agreement with earlier studies (Ref 8, 25).

The EDS spectrum of spark plasma sintered $Al_{10}Cr_{25}Co_{20}$-$Ni_{25}Fe_{20}$ HEA Alloy is shown in Fig. 8. It was concluded that the prepared HEAs consist of Al, Cr, Co, Ni and Fe metals. FCC phase was formed by Aluminums, Nickel and Cobalt constituents and BCC phase formed by Iron and Chromium. BCC and FCC biphase mixture was obtained and confirmed by XRD and EDS analysis.

3.3 Mechanical Behavior Analysis of Sintered HEAs Alloy

Figure 9(a), (b) shows stress–strain curves for $Al_{10}Cr_{25}$-$Co_{20}Ni_{25}Fe_{20}$ high-entropy alloy by conventional sintered samples at 1000 °C and 1200 °C and Spark plasma sintered samples at 1000 °C and 1200 °C. CoCuFeMnNi high-entropy alloy was fabricated by 50 h of MA and followed by SPS at 850 °C by M.A. Karimi et al (Ref 18) and yield tensile stress 318 MPa was achieved due to its denser microstructure. Mohanty et al. (Ref 28) synthesized AlCrCoFeNi HE As by MA and followed by SPS and obtained the compressive strength of 2.6 GPa. Fu et al. (Ref 29) fabricated Co20N-i20Fe20Al20Ti20 HEA by mechanical alloying and followed by SPS and obtained the compressive strength 2.9 GPa. Ji et al. (Ref 30) synthesized CoCrFeNiMn HEA through mechanical alloying and spark plasma sintering and obtained the compressive strength 1.9 GPa. These higher values were obtained by Mn, Ti content and presence of Ni_3Ti precipitates. In this

research work, the ultimate compressive stress for conventional sintering at 1000 °C and 1200 °C was 246 ± 5 MPa and 305 ± 6 MPa. Ultimate compressive strength of HEA for spark plasma sintered composite at 1000 °C and 1200 °C was

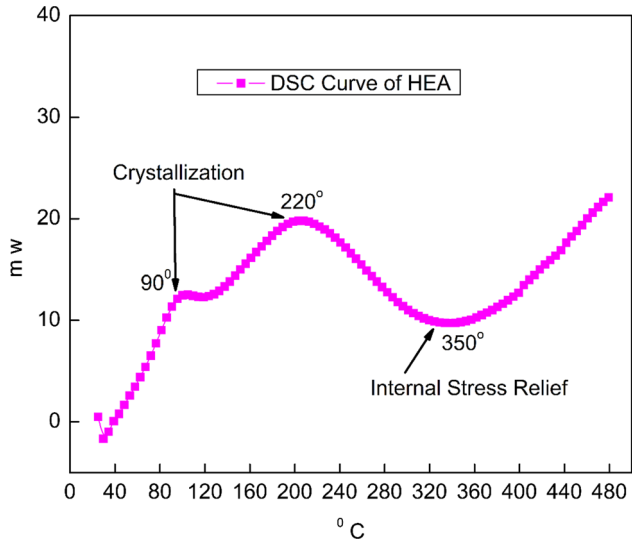

Fig. 7 DSC curve of prepared HEAs powder

369 ± 5 MPa and 442 ± 5 MPa and the total elongation was 17.7 ± 2%. Figure 9(b) shows stress–strain curves for $Al_{10}Cr_{25}Co_{20}Ni_{25}Fe_{20}$ high-entropy alloy by spark plasma sintered samples at 1000 °C and 1200 °C. Similar results was obtained by Maharana et al (Ref 31). Spark plasma sintering of $Ni_{46}Al_{12}Co_{18}Cr_8Fe_{12}Mo_4$ HEAs at 1100 °C resulted in improved densification, i.e., up to 99% and achieved excellent compressive yield strength of 1121 ± 21 MPa and elongation to failure up to 20 ± 1% attributed to the presence of ductile FCC phase (Ref 32). Figure 10 shows the densities of $Al_{10}Cr_{25}Co_{20}Ni_{25}Fe_{20}$ high-entropy alloy conventional sintered and spark plasma sintered samples. The experimental densities were 3.67 ± 0.5 and 4.39 ± 0.5 g/cm^3 for conventional sintering at 1000° and 1200 °C. The experimental densities were 5.8 ± 0.5 and 6.1 ± 0.5 g/cm^3 for SPSed samples at 1000° and 1200 °C. The relative density of the SPSed samples achieved was 97%. Figure 11 shows the Vickers microhardness values of $Al_{10}Cr_{25}Co_{20}Ni_{25}Fe_{20}$ high-entropy alloy conventional sintered and spark plasma sintered samples. For conventional sintering 135.1 ± 6 $HV_{0.5}$ for 1000 °C and 186.3 ± 8 $HV_{0.5}$ for 1200 °C values were obtained. For spark plasma sintering, 167 ± 5 $HV_{0.5}$ for 1000 °C and 212 ± 6 $HV_{0.5}$ for 1200 °C were obtained. Praveen et al (Ref 33) investigated the effect of molybdenum and niobium on CoCrFeNi HEAs and obtained the hardness value 570 HV. Liu et al. (Ref 34) fabricated CrMnFeCoNi HEAs through mechanical alloying

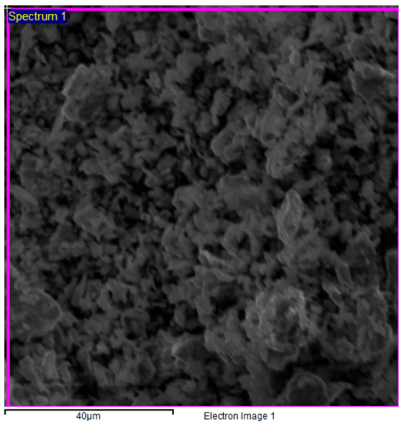

Element	Weight %	Atomic%
Al K	26.26	43.20
Cr K	4.23	3.61
Fe K	19.11	15.19
Co K	39.79	29.97
Ni K	10.61	8.02
Total	100.00	

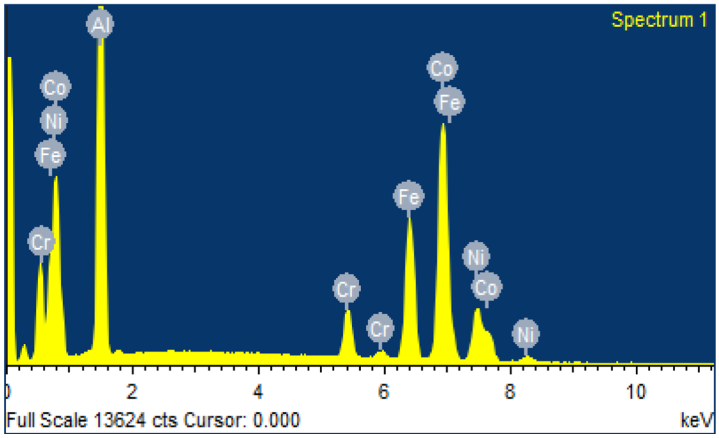

Fig. 8 EDS of spark plasma sintered $Al_{10}Cr_{25}Co_{20}Ni_{25}Fe_{20}$ HEA Alloy

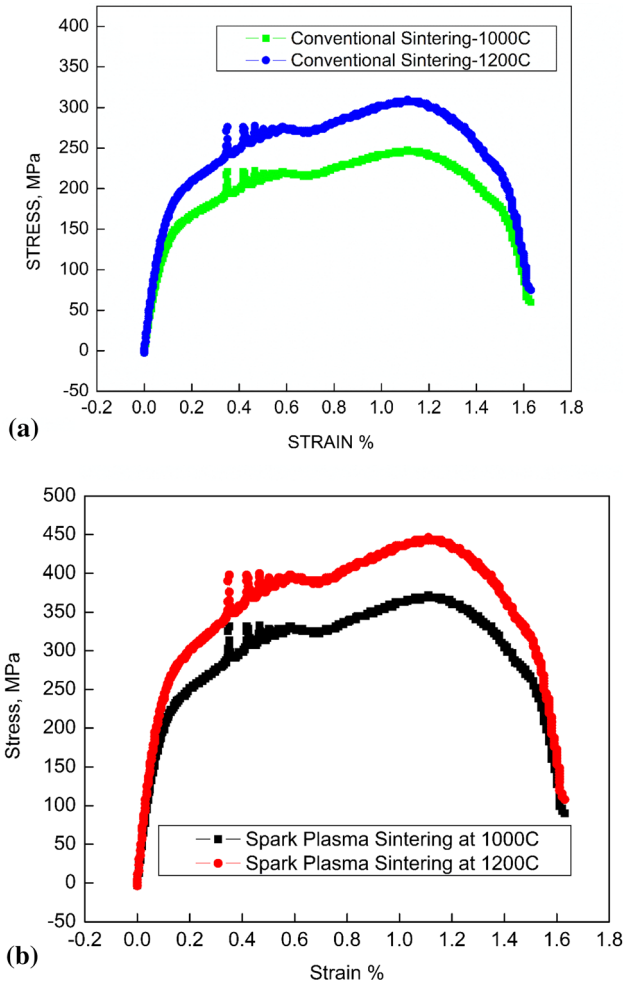

Fig. 9 Stress–Strain Curves for $Al_{10}Cr_{25}Co_{20}Ni_{25}Fe_{20}$ High-Entropy Alloy by (a) Conventional Sintered samples at 1000 °C & 1200 °C and (b) Spark Plasma Sintered samples at 1000 °C & 1200 °C

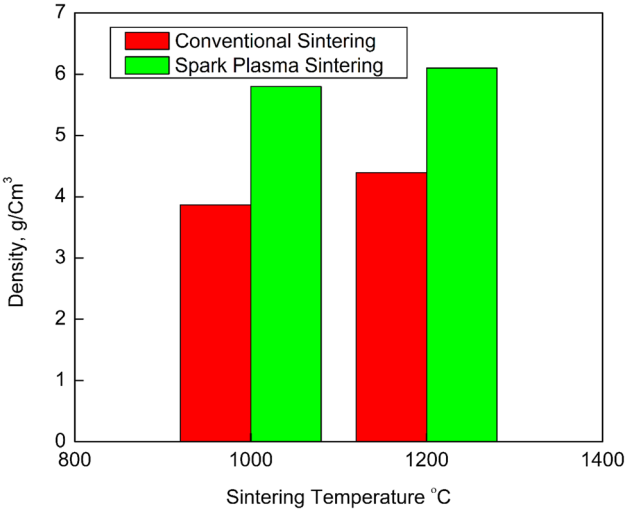

Fig. 10 The densities of $Al_{10}Cr_{25}Co_{20}Ni_{25}Fe_{20}$ High-Entropy Alloy for conventional sintered and spark plasma sintered samples

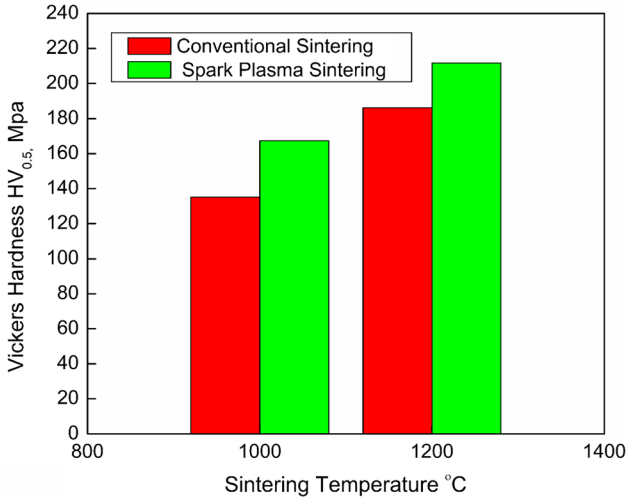

Fig. 11 The Vickers microhardness of $Al_{10}Cr_{25}Co_{20}Ni_{25}Fe_{20}$ High-Entropy Alloy for conventional and spark plasma sintered samples

and spark plasma sintering and obtained the hardness values of 526 HV. In this research work, the obtained hardness values were in good agreement with earlier studies (Ref 33, 34). Figure 12 shows electron backscattered diffraction analysis of sintered samples of $Al_{10}Cr_{25}Co_{25}Ni_{25}Fe_{20}$ high-entropy alloy. The HEAs which have BCC structures are strong, but non-flexible alloys, whereas HEAs with FCC structures are weak but flexible (Ref 29). The effect of sintering temperature and pressure on CoCrFeNiMo HEA was investigated by Aybuke Izci et al.(Ref 35) and reported that formation of BCC metastable, intermetallic and the FCC phases after 40 h of MA. Zhang et al (Ref 36) prepared AlCoCrFeNi HEA rapidly mixed 5 h and followed by spark plasma sintering at 1200 °C and obtained duplex BCC structure (ordered BCC & disordered BCC) and FCC Phases. In this research work , BCC and FCC biphase structure was obtained and was confirmed by Fig. 12. The mechanical properties of the SPSed HEA samples are given in Table 2.

4. Conclusion

$Al_{10}Cr_{25}Co_{20}Ni_{25}Fe_{20}$ high-entropy alloy powders were successfully fabricated by 30 h of MA. Sintering was done by conventional sintering and spark plasma sintering methods at 1000 °C and 1200 °C. Characterization of the as-milled powders by XRD and morphology analysis of as-milled powders by SEM and FETEM was done. The average crystallite size ~ 44 nm, the lattice strain 0.182 and the lattice parameter 0. 345 Å were obtained. BCC and FCC biphase mixture was obtained and confirmed by XRD, FETEM and EBSD analysis. Higher density, microhardness and compressive strength were obtained for spark plasma sintered samples compared with conventional sintered samples. Magnetic properties, thermal stability and wear studies of $Al_{10}Cr_{25}Co_{20}Ni_{25}Fe_{20}$ high-entropy alloy will be analyzed in the future study.

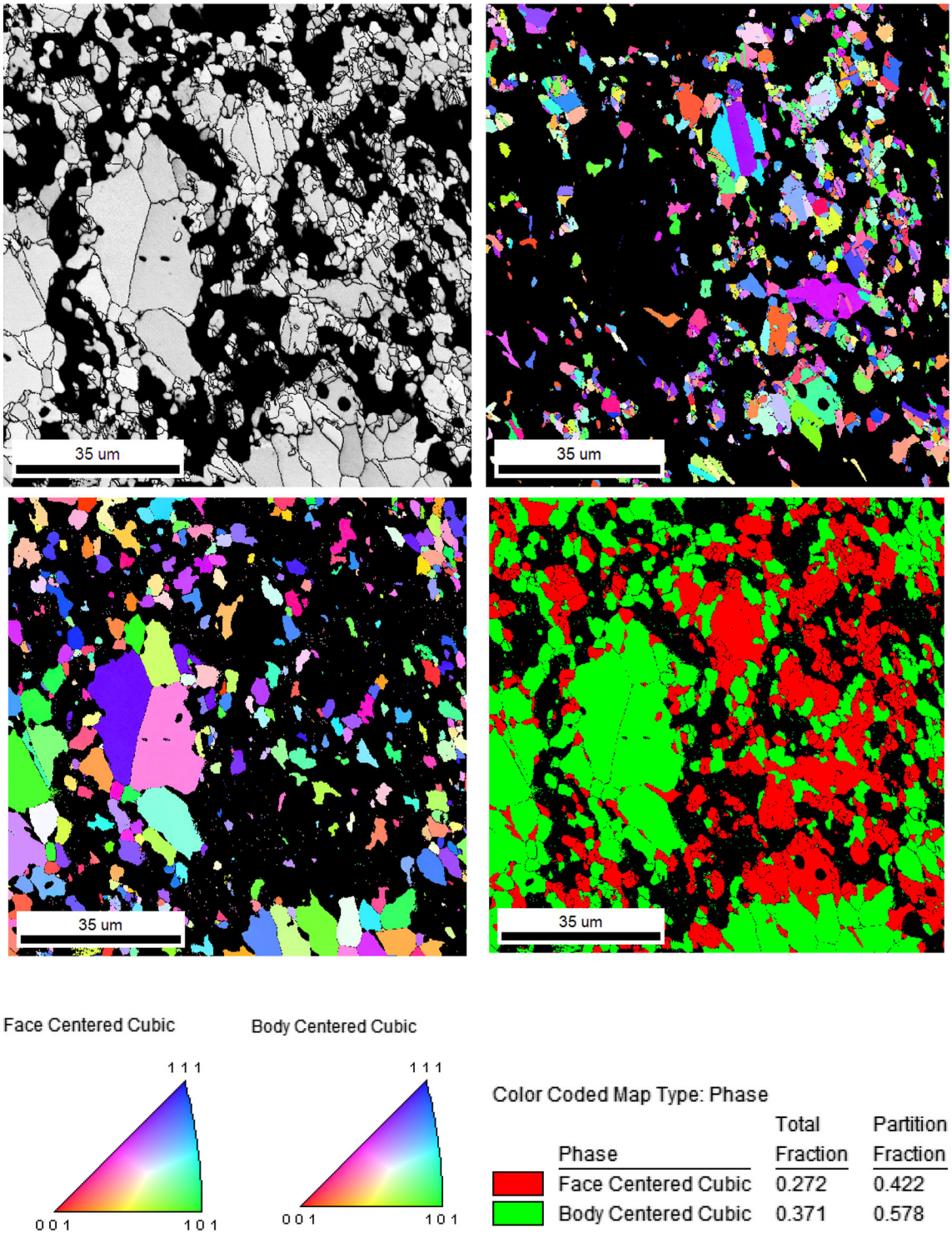

Fig. 12 EBSD Analysis of sintered samples of $Al_{10}Cr_{25}Co_{25}Ni_{25}Fe_{20}$ High-Entropy Alloy

Table 2 Mechanical parameters of the SPSed HEA

Sl. no.	Mechanical parameters	Values	
		Sintered at 1000 °C	Sintered at 1200 °C
1	Hardness ($HV_{0.5}$)	167 ± 5	212 ± 6
2	Ultimate compression strength, MPa	369 ± 5	442 ± 5
3	Yield strength, MPa	484 ± 6	530 ± 7
4	Ultimate tensile strength, MPa	597 ± 5	626 ± 5

Acknowledgment

This research work was supported by the seed money grant (Grant No:1018/Registrar/2022-23/Date:10.10.2022) received from the Management of the Periyar Maniammai Institute of Science & Technology, Thanjavur, Tamil Nadu, India.

Conflict of interest

The author declare that they have no known competing financial interests or personal relationships that could have appeared to influence the work reported in this paper.

References

1. J. Cao, B. Jiang, X. Cao, Z. Yuan, D. Yao, and J. Huang, High temperature oxidation resistance of an amorphous layer induced by ion implantation on the surface of Ni-based superalloy GH202, *Appl. Surf. Sci.*, 2022, **586**, p 152825. https://doi.org/10.1016/J.APSUSC.2022.152825
2. J. Cao, J. Zhang, R. Chen, Y. Ye, and Y. Hua, High temperature oxidation behavior of Nibased superalloy GH202, *Mater Charact*, 2016, **118**, p 122–128. https://doi.org/10.1016/J.MATCHAR.2016.05.013
3. J.W. Yeh, S.K. Chen, S.J. Lin, J.Y. Gan, T.S. Chin, T.T. Shun, C.H. Tsau, and S.Y. Chang, Nanostructured high-entropy alloys with multiple principal elements: novel alloy design concepts and outcomes, *Adv. Eng. Mater.*, 2004, **6**, p 299–303. https://doi.org/10.1002/adem.200300567
4. B. Cantor, I.T.H. Chang, P. Knight, and A.J.B. Vincent, Microstructural development in equiatomic multicomponent alloys, *Mater. Sci. Eng. A*, 2004, **375–377**, p 213–218. https://doi.org/10.1016/j.msea.2003.10.257
5. B.S. Murty, J.W. Yeh, S. Ranganathan, P.P. Bhattacharjee, High-entropy alloys: basic concepts, in: B.S. Murty, J.W. Yeh, S. Ranganathan, P.P.B.T.-H.-E.A. (Second E. Bhattacharjee (Eds.), Elsevier, 2019: pp. 13–30
6. O. Samoilova, N. Shaburova, A.O. Moghaddam, and E. Trofimov, Al0.25CoCrFeNiSi0.6 high entropy alloy with high hardness and improved wear resistance, *Mater. Lett.*, 2022, **328**, p 133190. https://doi.org/10.1016/j.matlet.2022.133190
7. B. Yin, Hu. Xiaojun, Lu. Zhaoping, and K. Chou, The effect of Ce addition on purification and inclusion modification of CoCrFeNiMn high entropy alloy, *J. Alloy. Compd.*, 2023, **934**, 167716. https://doi.org/10.1016/j.jallcom.2022.167716
8. X. Zhou, H. Dong, Y. Wang, and M. Yuan, Microstructure characteristics and mechanical performance of Fe-Cr-Ni- Al-Ti superalloy fabricated by powder metallurgy, *J. Alloy. Compd.*, 2022, **918**, 165612. https://doi.org/10.1016/j.jallcom.2022.165612
9. D. Yang, Y. Liu, T. Han, F. Zhou, Qu. Nan, M. Liao, Z. Lai, and J. Zhu, High thermal stability and oxidation behavior of FeCrNiAl-based medium-entropy alloys prepared by powder metallurgy, *J. Alloy. Compd.*, 2022, **918**, 165562. https://doi.org/10.1016/j.jallcom.2022.165562
10. A.S. Rogachev, S.G. Vadchenko, DYu. Kovalev, N.A. Kochetov, M. Zhukovskyi, T. Orlova, and A.S. Mukasyan, Long term stability of a high-entropy CoCrFeNiTi alloy fabricated by mechanical alloying, *J. Alloy. Compd.*, 2023, **931**, 167470. https://doi.org/10.1016/j.jallcom.2022.167470
11. H. Kalantari, M. Zandrahimi, M. Adeli, and H. Ebrahimifar, The production of nanocrystalline AlCoCrFeNiTiZn high entropy alloy via mechanical alloying: Study of the formation mechanism, microstructural evolution, and magnetic properties of the alloy, *Intermetallics*, 2022, **150**, 107694. https://doi.org/10.1016/j.intermet.2022.107694
12. Q. Cheng, J. Chen, Yu. Gewen Yi, Y.G. Shan, J. Wang, and W. Wang, Comparative study of the microstructure and phase evolution of FeCoCrNiAl high-entropy alloy-matrix WC nanocomposite powders prepared by mechanical alloying, *J. Alloy. Compd.*, 2023, **938**, 168518. https://doi.org/10.1016/j.jallcom.2022.168518
13. M.R. Toroghinejad, F. Ebrahimi, and A. Shabani, Synthesis of the AlCrCuMnNi high entropy alloy through mechanical alloying and spark plasma sintering and investigation of its wear behavior, *J. Mater. Res. Technol.*, 2022, **21**, p 3262–3273. https://doi.org/10.1016/j.jmrt.2022.10.120
14. M.A. Karimi, M. Shamanian, M.H. Enayati, M. Adamzadeh and M. Imani, Fabrication of a novel magnetic high entropy alloy with desirable mechanical properties by mechanical alloying and spark plasma sintering, *J. Manuf. Process.*, 2022, **84**, p 859–870. https://doi.org/10.1016/j.jmapro.2022.10.048
15. Y. Fei Gao, L.H. Sun, J. Shen, W. Liu, M. Ba, and C. Deng, Microstructure and strengthening mechanisms of novel lightweight TiAlV05CrMo refractory high-entropy alloy fabricated by mechanical alloying and spark plasma sintering, *J. Alloys Compd.*, 2023, **932**, p 167659. https://doi.org/10.1016/j.jallcom.2022.167659
16. M.R. Toroghinejad, H. Pirmoradian, and A. Shabani, Synthesis of FeCrCoNiCu high entropy alloy through mechanical alloying and spark plasma sintering processes, *Mater. Chem. Phys.*, 2022, **289**, p 126433. https://doi.org/10.1016/j.matchemphys.2022.126433
17. H. Jain, Y. Shadangi, D. Chakravarty, A.K. Dubey, and N.K. Mukhopadhyay, High entropy steel processed through mechanical alloying and spark plasma sintering: alloying behaviour, thermal stability and mechanical properties, *Mater. Sci. Eng. A*, 2022, **856**, p 144029. https://doi.org/10.1016/j.msea.2022.144029
18. A. Shahbazkhan, H. Sabet, and M. Abbasi, Microstructural and mechanical properties of NiCoCrAlSi high entropy alloy fabricated by mechanical alloying and spark plasma sintering, *J. Alloy. Compd.*, 2022, **896**, 163041. https://doi.org/10.1016/j.jallcom.2021.163041
19. A. Olejarz, W.Y. Huo, M. Zieliński, R. Diduszko, E. Wyszkowska, A. Kosińska, D. Kalita, I. Jóźwik, and M. Chmielewski, Microstructure and mechanical properties of mechanically-alloyed CoCrFeNi high-entropy alloys using low ball-to-powder ratio, *J. Alloys Compd.*, 2023, **938**, p 168196. https://doi.org/10.1016/j.jallcom.2022.168196
20. J.M. Torralba, P. Alvaredo, and A. García-Junceda, High-entropy alloys fabricated via powder metallurgy, *Critic. Rev. Powder Metall.*, 2019, **62**(2019), p 84–114. https://doi.org/10.1080/00325899.2019.1584454
21. C. Nagarjuna, S.K. Dewangan, H. Lee, K. Lee, and B. Ahn, Exploring the mechanical and tribological properties of AlCrFeNiTi high-entropy alloy fabricated by mechanical alloying and spark plasma sintering, *Vacuum*, 2023, **218**, p 112611. https://doi.org/10.1016/j.vacuuam.2023.112611
22. K. Zhang and Fu. Zhengyi, Effect of annealing treatment on phase composition and microstructure of CoCrFeNiTiAlx high entropy alloys, *Intermetallics*, 2012, **22**, p 24–32. https://doi.org/10.1016/j.intermet.2011.10.010
23. A. Shabani, M.R. Toroghinejad, and A. Shafyei, Log_e RE microstructure and mechanical properties of a multiphase FeCrCuMnNi high-entropy alloy, *J. Mater. Eng. Perform.*, 2019, **28**, p 2388–2398
24. G.K. Williamson and W.H. Hall, x-Ray line broadening from field aluminum and wolfram, *Acta Metall.*, 1953, **1**(1), p 22–31
25. Yu. Fei Gao, L.H. Sun, J. Shen, W. Liu, M. Ba, and C. Deng, Microstructural evolution and thermal stability in a nanocrystalline lightweight TiAlV0.5CrMo refractory high-entropy alloy synthesized by mechanical alloying, *Mater. Lett.*, 2022, **329**, p 133179. https://doi.org/10.1016/j.matlet.2022.133179
26. B. Ren, S. Li, N. Wang, Z. Xiao, E. Axinte, and Y. Wang, Excellent catalytic performance of mechanically alloyed $AlCrFeMnTiZr_{0.5}$ high-entropy alloy for malachite green degradation, *Mater. Lett.*, 2023, **328**, p 133076. https://doi.org/10.1016/j.matlet.2022.133076
27. H. Jain, Y. Shadangi, D. Chakravarty, A.K. Dubey, and N.K. Mukhopadhyay, High entropy steel processed through mechanical alloying and spark plasma sintering: alloying behavior, thermal stability and mechanical properties, *Mater. Sci. Engg. A*, 2022, **856**, p 144029. https://doi.org/10.1016/j.msea.2022.144029
28. S. Mohanty, T.N. Maity, S. Mukhopadhyay, S. Sarkar, N.P. Gurao, and S. Bhowmick, Krishanu biswas, powder metallurgical processing of equiatomic AlCoCrFeNi high entropy alloy: microstructure and mechanical properties, *Mater. Sci. Engg. A*, 2017, **679**, p 299–313. https://doi.org/10.1016/j.msea.2016.09.062
29. Fu. Zhiqiang, W. Chen, H. Wen, S. Morgan, F. Chen, B. Zheng, Y. Zhou, L. Zhang, and E.J. Lavernia, Microstructure and mechanical behavior of a novel Co20Ni20Fe20Al20Ti20 alloy fabricated by mechanical alloying and spark plasma sintering, *Mater. Sci. Engg. A*, 2015, **644**, p 10–16. https://doi.org/10.1016/j.msea.2015.07.052
30. W. Ji, W. Wang, H. Wang, J. Zhang, Y. Wang, F. Zhang, and Fu. Zhengyi, Alloying behavior and novel properties of CoCrFeNiMn high-entropy alloy fabricated by mechanical alloying and spark plasma

sintering, *Intermetallics*, 2015, **56**, p 24–27. https://doi.org/10.1016/j.intermet.2014.08.008
31. D.K.V.D. Sudhansu Maharana, S.A. Prasad, M.S. Seetharaman, and T. Laha, Effect of sintering parameters on phase evolution, microstructural development and mechanical behavior of Ni46Al12Co18Cr8-Fe12Mo4 high entropy alloy synthesized via mechanical alloying and spark plasma sintering, *Mater. Sci. Engg. A*, 2023, **886**, p 145695. https://doi.org/10.1016/j.mesa.2023.145695
32. M. Zeraati, M.H.K. Feizabad, and G.R. Khayati, An investigation of the magnetic, mechanical, and kinetic characteristics of CuCrFeTiNi high entropy alloy by mechanical alloying and spark plasma sintering, *J. Alloys Compd.*, 2023, **958**, p 170347. https://doi.org/10.1016/j.jallcom.2023.170347
33. S. Praveen, B.S. Murty, and R.S. Kottada, Effect of molybdenum and niobium on the phase formation and hardness of nanocrystalline CoCrFeNi high entropy alloys, *J. Nanosci. Nanotechnol.*, 2014, **14**(10), p 8106–8109. https://doi.org/10.1166/jnn.2014.9441
34. Y. Liu, J. Wang, Q. Fang, B. Liu, Wu. Yuan, and S. Chen, Preparation of superfine-grained high entropy alloy by spark plasma sintering gas atomized powder, *Intermetallics*, 2016, **68**, p 16–22. https://doi.org/10.1016/j.intermet.2015.08.012
35. A. Izci, B. Yavas, I. Antoniac et al., Investigation of the effects of spark plasma sintering parameters on equiatomic CoCrFeNiMo high entropy alloy, *J. of Mater. Engg. and Perform.*, 2023 https://doi.org/10.1007/s11665-023-08872-8
36. A. Zhang, J. Han, J. Meng et al., Rapid preparation of AlCoCrFeN high entropy alloy by spark plasma sintering from elemental powder misxture, *Mater. Lett.*, 2016, **181**, p 82–85. https://doi.org/10.1016/j.matlet.2016.06.014